



HAL
open science

Effect of water incorporation on the ionic conduction properties of the solid electrolyte material RbTiO.(HO)

Sofia de Sousa Coutinho, David Bérardan, Guillaume Lang, Rémi Federicci, Paola Giura, Keevin Beneut, Nita Dragoe, Stéphane Holé, Brigitte C. Leridon

► To cite this version:

Sofia de Sousa Coutinho, David Bérardan, Guillaume Lang, Rémi Federicci, Paola Giura, et al.. Effect of water incorporation on the ionic conduction properties of the solid electrolyte material RbTiO.(HO). Solid State Ionics, 2021, 364, pp.115630. 10.1016/j.ssi.2021.115630 . hal-03377781

HAL Id: hal-03377781

<https://hal.science/hal-03377781>

Submitted on 26 Nov 2021

HAL is a multi-disciplinary open access archive for the deposit and dissemination of scientific research documents, whether they are published or not. The documents may come from teaching and research institutions in France or abroad, or from public or private research centers.

L'archive ouverte pluridisciplinaire **HAL**, est destinée au dépôt et à la diffusion de documents scientifiques de niveau recherche, publiés ou non, émanant des établissements d'enseignement et de recherche français ou étrangers, des laboratoires publics ou privés.

Effect of water incorporation on the ionic conduction properties of the solid electrolyte material $\text{Rb}_2\text{Ti}_2\text{O}_5 \cdot (\text{H}_2\text{O})_x$

Sofia de Sousa Coutinho^{*1}, David Bérardan², Guillaume Lang¹, Rémi Federicci¹, Paola Giura³, Keevin Beneut³, Nita Dragoe², Stéphane Holé¹ and Brigitte Leridon¹

¹ LPEM – ESPCI Paris – PSL University – Sorbonne Université – CNRS – 10 rue Vauquelin – 75005 Paris – France

² ICMMO – CNRS – Université Paris-Saclay – rue du doyen Georges Poitou – 91405 Orsay cedex – France

³ IMPMC – Sorbonne Université – 4 place Jussieu – 75005 Paris – France

Abstract

Previous work has demonstrated the accumulation of negative charges on the anode side of the ion conductor $\text{Rb}_2\text{Ti}_2\text{O}_5$ when placed under voltage between two metallic electrodes. The nature of these accumulated species and of the conducting ions is investigated by a combination of thermogravimetric analysis (TGA), X-ray diffraction, dielectric response measurements, charge distribution, IR absorption spectroscopy and nuclear magnetic resonance (NMR) measurements. TGA shows that the as-grown samples have incorporated a considerable amount of water (up to 0.35 H_2O per unit cell) that is eliminated at two different temperature thresholds. However, no significant variation of the lattice parameters is observed by X-Ray diffraction. A strong dependence of the dielectric properties and of the accumulated charge density on the water content is demonstrated. All the results point toward a mechanism of proton and hydroxide conduction associated with a change of valence for titanium.

Keywords: superionic conductor, solid electrolyte, Rubidium dititanate, Potassium dititanate, virtual cathode, supercapacitor material

2010 MSC: 00-01, 99-00

1. Introduction

Previous studies have demonstrated remarkable dielectric properties in the rubidium dititanate $\text{Rb}_2\text{Ti}_2\text{O}_5$ (RTO) [1] and to a smaller extent in $\text{K}_2\text{Ti}_2\text{O}_5$ (KTO) [2] which are part of the same $\text{M}_2\text{Ti}_2\text{O}_5$ (MTO) family of materials where $\text{M} = \{\text{H}, \text{K}, \text{Na}, \text{Rb}, \text{Cs}\}$. RTO presents a notably high ionic conductivity between 200 K and 300 K leading to an equally high polarization and a colossal equivalent permittivity of about 10^9 at 270 K and at low frequency [1]. This is three to four orders of magnitude above state-of-the-art values for permittivity at low frequency. These properties were ascribed to a high ionic mobility ($\sigma = 10^{-3} \text{ S.cm}^{-1}$

*Corresponding Author

Email address: sofia.de-sousa-coutinho@espci.fr (Sofia de Sousa Coutinho^{*1}, David Bérardan², Guillaume Lang¹, Rémi Federicci¹, Paola Giura³, Keevin Beneut³, Nita Dragoe², Stéphane Holé¹ and Brigitte Leridon¹)

at 270 K in RTO) together with a negligible electronic conductivity. However, the high value of the ionic conductivity *per se* is not sufficient to account for the creation of such a high equivalent permittivity.

10 In a more recent work [3, 4], charge distribution measurements using the Pressure-Wave-Propagation (PWP) method were performed on metal-RTO-metal (MIM) type samples, with gold as the metal. The results highlighted the presence of negative charges that accumulate at the anode interface inside the material under an applied voltage. Remarkably enough, no positive charge was observed near the cathode interface and the electric field was found to be nil inside the material, indicating the creation of
15 a virtual cathode [3, 4]. These findings thus raised the question of the nature of the mobile ionic species at play inside the material. The very high value of the permittivity as well as the potential applications of $\text{Rb}_2\text{Ti}_2\text{O}_5$ in supercapacitors or memristive devices motivate the understanding of the microscopic dynamics taking place inside the material and of the external parameters influencing its properties.

In the literature, the effect of water incorporation on oxide properties has been intensively investigated
20 [5, 6, 7]. In particular, in most oxygen vacancy-dominated oxides, water incorporation leads to proton introduction as hydroxide defects as follows:



where $\text{V}_\text{O}^\bullet$ represents oxygen vacancies, O_O^\times represents oxygen sites in the material matrix and $(\text{OH})_\text{O}$ represent hydroxide ions occupying oxygen sites [8, 9], according to the notation of Kröger and Vink [10]. In addition, it is known that lamellar oxides such as MTO are prone to water intercalation [11, 12,
25 13, 14]. Part of the intercalated water molecules experience ion dissociation. In addition, the presence of undissociated water molecules will enable a Grotthuss mechanism for proton conduction [15] or even for hydroxide conduction [16].

In this article, the sample synthesis and preparation protocol is first detailed before presenting the results obtained by a combination of thermogravimetric analysis (TGA), X-ray diffraction, dielectric response
30 measurements, charge distribution measurements, IR absorption spectroscopy and nuclear magnetic resonance (NMR) spin-lattice relaxation measurements. All the obtained results enable to demonstrate the leading role of water incorporation in the ionic conduction and dielectric properties of RTO material. In particular, the results demonstrate the strong dependence of the amount of charges present inside the material on the water content, and points towards hydroxide ion OH^- as responsible for the
35 negative charge that builds up under voltage near the cathode, either by depletion of the protons or by accumulation of hydroxide ions, or even by addition of both mechanisms.

2. Experiments and Results

2.1. Synthesis and sample preparation

All $\text{Rb}_2\text{Ti}_2\text{O}_5$ powders were prepared using a standard solid-state reaction route. First TiO_2 (> 99.8%)
40 and RbNO_3 (> 99.9%) powders were weighed, with 15 % excess of RbNO_3 , in order to obtain the de-

sired stoichiometry for the final compound. Then, the powders were mixed and calcinated at 930°C for 3 hours in a platinum crucible in laboratory atmosphere. $\text{Rb}_2\text{Ti}_2\text{O}_5$ crystals were obtained after decreasing the temperature at a cooling rate of $0.1\text{ }^\circ\text{C}\cdot\text{h}^{-1}$ to 880°C and then at $3\text{ }^\circ\text{C}\cdot\text{h}^{-1}$ to room temperature.

For dielectric measurements, a 350°C-dehydrated RTO ceramic sample was obtained from as-grown
45 crystals ground and dehydrated under O_2 atmosphere at 350°C. The ceramic sample was prepared in a glove box under N_2 atmosphere by applying a pressure of $6\text{ tons}\cdot\text{cm}^{-2}$ in a 13-mm diameter die. Gold electrodes were then vacuum deposited and aluminum foils were finally pasted with silver lacquer in order to ensure a good and robust electrical coupling.

For PWP measurements, RTO ceramic samples were obtained from as-grown crystals ground and de-
50 hydrated separately under O_2 atmosphere at 120°C, 150°C, 350°C and 820°C. For each dehydration temperature, two ceramic samples were prepared in glove box under N_2 atmosphere by applying a pressure of $6\text{ tons}\cdot\text{cm}^{-2}$ in a 13-mm diameter die. The RTO ceramic samples thus obtained were 1.2 to 1.7 mm thick. Gold electrodes were then vacuum deposited and $10\text{-}\mu\text{m}$ -thick gold foils were finally pasted with silver lacquer in order to ensure a good mechanical and electrical coupling. Samples were measured
55 successively in the same set-up while immersed inside anhydrous silicone oil (except for the as-grown samples) in order to maintain their dehydration state. The typical structure of each sample is depicted in Fig. 1. At each step between the dehydration of the crystal and the measurement of the ceramics, special care was taken to minimize the exposure of the samples to the atmosphere.

For all samples, dehydration treatments were performed inside in a TGA analyzer under anhydrous
60 atmospheres. Samples were then transferred into a glove box. The transfer time between the TGA chamber and the glove box is one minute at most. As will be shown below, samples are shown to spontaneously hydrate when exposed to ambient atmosphere. However by referring to the TGA curve relative to the kinetics of hydration of an RTO powder (Fig. 2), one can estimate that only 0.001 molecule of water per formula unit ($\text{Rb}_2\text{Ti}_2\text{O}_5\cdot(\text{H}_2\text{O})_{0.001}$) is likely to be incorporated into the sample during the
65 transfer from the dehydration chamber to the glove box. Gold deposition was done in an evaporation chamber, outside the glove box. The transfer time, added to the primary vacuum time, is approximately 10 minutes, which corresponds to nearly 0.006 molecule of water per formula unit ($\text{Rb}_2\text{Ti}_2\text{O}_5\cdot(\text{H}_2\text{O})_{0.006}$) incorporated within the sample, which is negligible as compared to the values observed for hydrated or as-grown samples typically of the order of 0.05 to 0.5 molecule of water per formula unit.

70 For IR absorption measurements, the sample was obtained from a mixture of 99 % KBr and 1 % $\text{Rb}_2\text{Ti}_2\text{O}_5$ ground manually in a mortar and pelletized under vacuum for 10 minutes. A so-called reference pellet composed of 100 % KBr was produced in order to be able to extract the IR absorption component only linked to $\text{Rb}_2\text{Ti}_2\text{O}_5$. In order to ensure the homogeneity and similarity of the powders making the pellets, the KBr of the reference pellet was ground with the same intensity and during the same period
75 as the KBr and $\text{Rb}_2\text{Ti}_2\text{O}_5$ mixture.

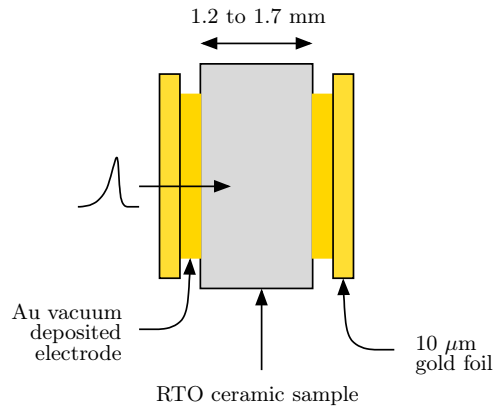


Figure 1: Scheme of a typical RTO ceramic sample structure used for PWP measurements.

2.2. Thermogravimetric Analysis (TGA)

Thermogravimetric analyses were performed on RTO powder using a Setaram Setsys Evo thermogravimetric analyzer, using amorphous SiO_2 crucibles, under various atmospheres. For each measurement, a blank was first measured using an empty crucible, in the same experimental conditions (gas flow and heating rate). The signal corresponding to the dehydration of the sample was then obtained by subtracting the blank signal to the raw measurement.

A typical TGA curve of an as-grown sample is displayed in Fig. 2. It exhibits two distinct features: a significant weight loss between room temperature and circa 300°C and a second one between 700°C and 820°C . During the first stage of heating, between room temperature and about 300°C , 4 to 5 % weight loss were observed depending on samples (it should be noted that part of this weight loss occurred at room temperature during the purge of the measurement chamber). A second loss of about 0.6-0.8 % depending on samples is measured between about 700°C and 820°C . Both processes are irreversible, as no feature is observed in the cooling curve. However, they are restored if the samples are exposed to the laboratory atmosphere.

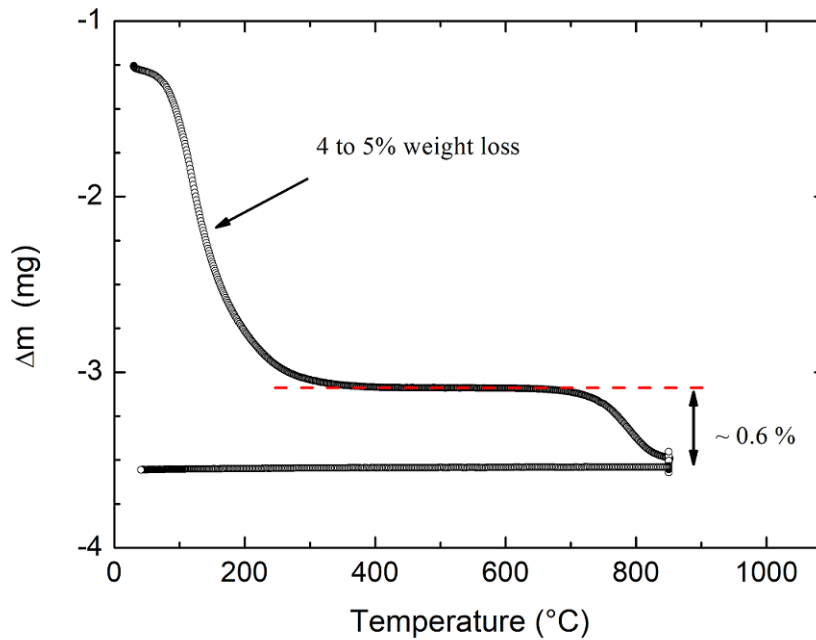


Figure 2: Representative example of a thermogravimetric curve obtained when heating an as-grown RTO powder under oxygen with a heating rate of 10 K/min. Note: the weight loss does not begin at 0 mg as significant losses already occurred during the purge of the analysis chamber.

90 In order to identify the volatile content present within the samples which are lost during heating, temperature cycling under different atmospheres was carried out. The experimental protocol is as follows: a first heating in a pure oxygen atmosphere is carried out on an as-grown RTO powder at 850°C. A TGA curve identical to the one in Fig. 2 is obtained. Once the mass has stabilized, the measurement chamber is purged and switched to flowing argon ($P(\text{O}_2) = 10^{-5}$ atm). After 8 h, the chamber is purged and

95 switched to flowing oxygen. Last, after 8 h, the chamber is switched again to flowing argon (Fig. 3). As it can be seen in Fig. 3, there is almost no effect of the oxygen partial pressure (between 1 atm and 10^{-5} atm) on the mass of the samples. It means that oxygen vacancies concentration is not the main parameter explaining the difference of transport properties between the samples. Note that it does not

100 mean that no oxygen vacancies are present or that their concentration is negligible, but only that oxygen concentration does not change between $P(\text{O}_2) = 1$ atm and $P(\text{O}_2) = 10^{-5}$ atm. The analysis chamber is then purged before exposing the sample to an atmosphere of pure CO_2 for one hour at room temperature. Then temperature cycling in a pure oxygen atmosphere is carried out. The TGA curve of Fig. 4 is

105 obtained. If the loss of mass at high temperatures of an as-grown sample was due to de-carbonation, we should see a mass variation of the sample at a given temperature in Fig. 4 because carbon dioxide would be reincorporated during the exposure to pure CO_2 atmosphere at room temperature. These results enable to rule out the possible contribution to the formation of oxygen vacancies and to the de-carbonation of the samples in the mass losses observed during heating in Fig. 2.

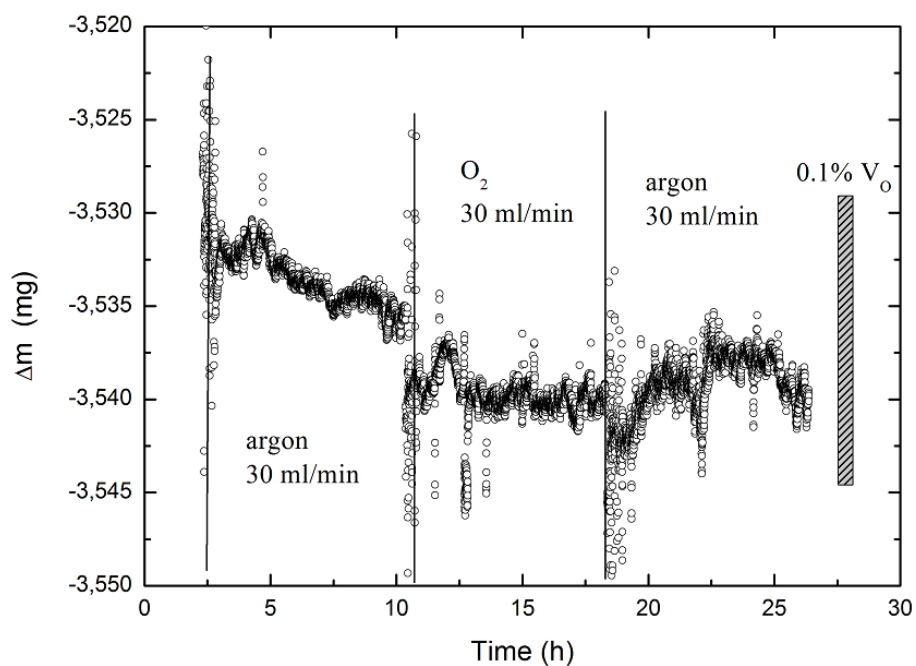


Figure 3: TGA curve (blank subtracted) obtained by cycling a dehydrated sample at 850°C between $P(O_2) = 1 \text{ atm}$ (O_2 flow) and $P(O_2) = 10^{-5} \text{ atm}$ (Ar flow). The height of the gray surface corresponds to the magnitude of the weight change that would be expected by the formation-suppression of 0.1 % oxygen vacancies (for example between $Rb_2Ti_2O_5$ and $Rb_2Ti_2O_{4.995}$).

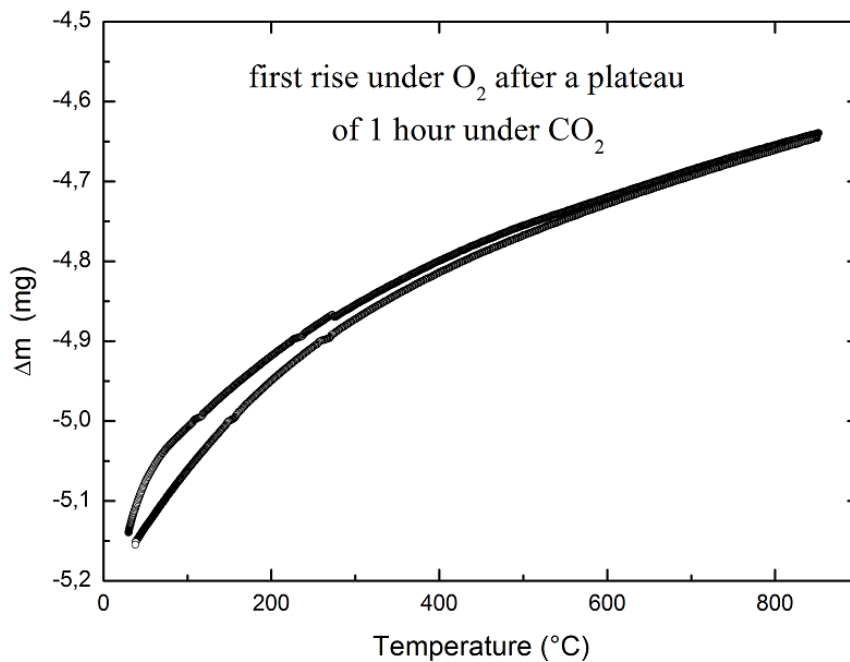


Figure 4: TGA curve obtained during a third rise under O_2 atmosphere after the sample being exposed to an atmosphere of pure CO_2 for one hour at room temperature (no blank subtracted).

Therefore, the very significant losses observed when heating as-grown samples, or dehydrated samples

stored in ambient conditions, under O₂ atmosphere can be unambiguously attributed to water losses.

110 The temperature range of the first feature observed during heating was perfectly reproducible from one sample to another. However, the precise weight loss was difficult to estimate, as part of the dehydration occurred at room temperature during the purge of the measurement chamber. Besides, the hydration level of different as-grown samples could be different due to different air exposure or different humidity level during the synthesis. Therefore, a different TGA process was used. An as-grown sample was first

115 heated at 550°C under oxygen during 4 h to ensure a complete elimination of the “loosely bound” water. It was then cooled down to room temperature, and the measurement chamber was opened so as to measure the weight gain of the sample during rehydration. The resulting TGA curve is plotted in Fig. 5. A more or less parabolic evolution of the mass of the sample can be observed, which is a signature of a diffusion-limited process. The rapid and significant weight gain confirms the very hygroscopic

120 character of the material.

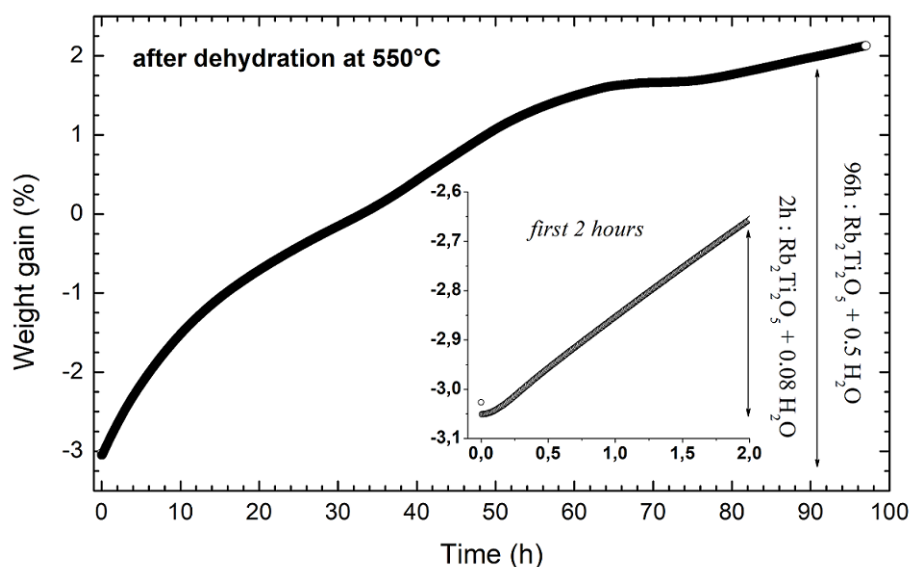


Figure 5: Weight gain observed during the rehydration of a sample, previously dehydrated at 550°C during 4 h.

2.3. Powder XRD measurements

The X-ray powder diffraction (XRD) patterns were recorded using an XPert Pro Analytical diffractometer equipped with a Cu K α radiation source ($K\alpha_1 = 1.540562 \text{ \AA}$) and an XCelerator detector. XRD measurements were performed along the following protocol: an as-grown RTO powder was dehydrated at

125 810°C for 4 hours under flow of O₂ leading in principle to total or almost total dehydration. The sample was then transferred to a glove box, spending a maximum of 2 mn in the laboratory atmosphere. It was placed inside a spinner type sample holder with a polymer dome clamped on an O-ring, filled in the glove box, in order to avoid rehydration during the acquisition. A first diffractogram was measured by integrating over a full night in order to obtain a good statistic. Then, the sample holder was opened

130 and left exposed to air for 9 hours. If we assume that rehydration was occurring at the same rate as

the previous TGA analyzes (Fig. 2), we can estimate the gain in mass at around 1.4 % by mass which corresponds to more than 0.1 molecule of water per formula unit of $\text{Rb}_2\text{Ti}_2\text{O}_5$. New acquisition of a diffractogram under exactly the same conditions was performed. The two diffractograms obtained respectively for the 810°C dehydrated sample and after subsequent 9-hours-exposure to air are shown in Fig. 6.

Lebail refinements were performed with the FullProf suite of programs on the two X-ray powder diffraction patterns recorded in Bragg-Brentano geometry. The background was modeled using a linear interpolation between a set of background points and a Pseudo-Voigt function was used for peak shape functions. Table 1 displays the lattice parameters deduced from Lebail refinements performed on the X-ray Powder Pattern. It appears that no significant changes are observed in the unit cell parameters, which seems highly surprising. These results were repeated several times leading to the same observation.

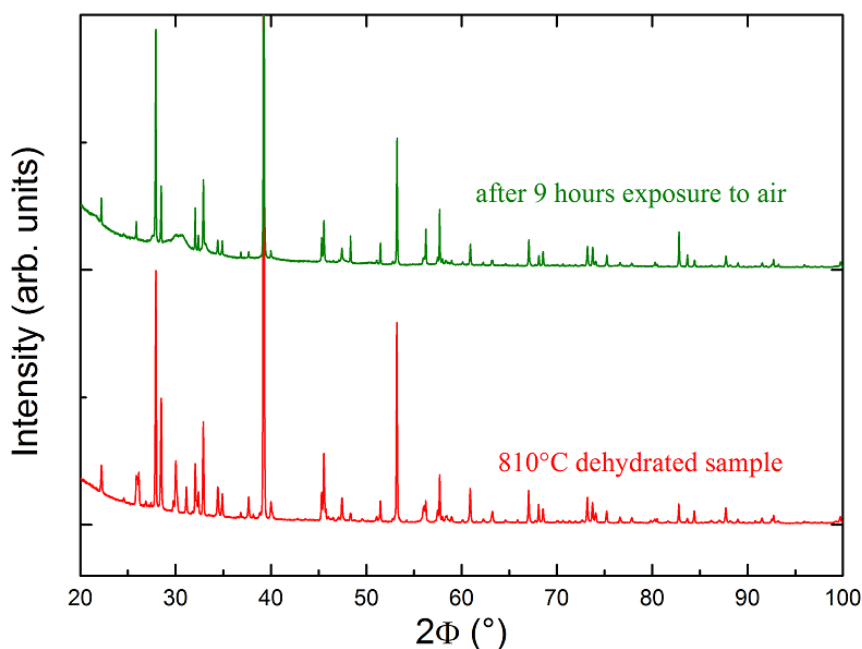


Figure 6: Diffractograms acquired on a 810°C dehydrated sample (red line) and after 9 hours exposure to air (green line).

	dehydrated sample	after 9 hours exposure to air
Space Group	$C2/m$	$C2/m$
a (Å)	11.3363(2)	11.3360(1)
b (Å)	3.8373(1)	3.8271(5)
c (Å)	6.9898(1)	6.9904(4)
β (°)	100.280(9)	100.275(5)
Volume (Å ³)	298.362(3)	298.401(6)
R_{Bragg} (%)	6.80	8.75

Table 1: Results of the Le Bail Refinement on the X-ray Powder Pattern of the 810°C dehydrated sample and after 9 hours exposure to air.

2.4. Dielectric response measurements

Dielectric response measurements were performed using Solartron 1296 Dielectric interface and 1260
145 impedance/gain analyzer both controlled by SMarT software. Real and imaginary parts of the equivalent impedance Z were measured as a function of frequency from 10^6 Hz to 10^{-1} Hz under an ac-voltage of 100 mV. Real and imaginary parts of the equivalent relative permittivity were obtained from the impedance knowing the thickness and the area of each RTO ceramic samples, as reported in Eq.(2) :

$$\text{Re}(\epsilon_r) = \frac{\text{Re}(1/Z \omega) d}{A \epsilon_0} \quad \text{and} \quad \text{Im}(\epsilon_r) = \frac{\text{Im}(1/Z \omega) d}{A \epsilon_0}, \quad (2)$$

where $\epsilon_0 = 8,854.10^{-12}$ F.m⁻¹ is the permittivity of the vacuum, d the thickness, A the area of the RTO
150 ceramic sample and ω is the circular frequency. The values of the real part of the admittivity were then extracted from the real and imaginary parts of the complex impedance as follows:

$$\text{Re}(Y) = \frac{d}{A} \left(\frac{\text{Re}(Z)}{\text{Re}(Z)^2 + \text{Im}(Z)^2} \right). \quad (3)$$

Dielectric measurements were performed on both as-grown and 350°C-dehydrated RTO ceramic samples. For the latter one, the dielectric measurements were carried out inside a glove box to minimize exposure to ambient atmosphere. Results are displayed in Fig. 7 and 8.

155 In Fig. 7, the real and imaginary parts of equivalent complex permittivity ϵ_r are plotted as a function of frequency for the two samples. For the as-grown RTO sample, the behavior of $\text{Re}(\epsilon_r)$ and $\text{Im}(\epsilon_r)$ is consistent with previous observations [1, 2]. The apparent relative permittivity of about 10^9 at low frequency is comparable to the values obtained for RTO single crystals [1]. Below 1 Hz, a capacitive plateau seems to be reached, indicating the onset of local charge accumulation taking place at the ion-
160 blocking electrode as reported in [3, 4]. For the 350°C-dehydrated RTO sample, a similar curve behavior is obtained with a shift of almost 4 decades towards the low frequencies of $\text{Re}(\epsilon_r)$ and $\text{Im}(\epsilon_r)$ compared to the as-grown sample.

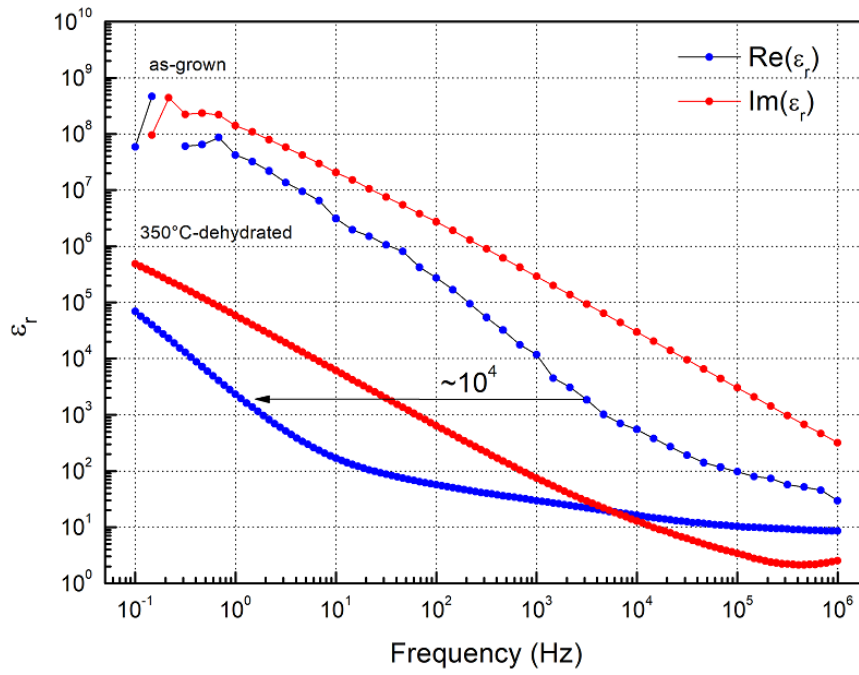


Figure 7: Real part (blue dots) and imaginary part (red dots) of the equivalent permittivity as function of frequency for the as-grown and the 350°C-dehydrated RTO samples.

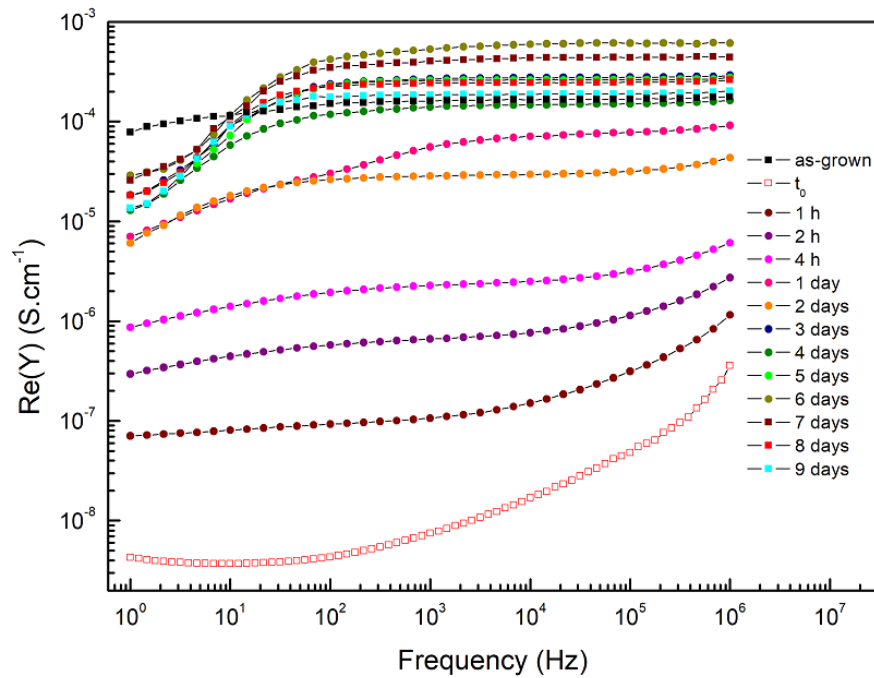


Figure 8: Impact of air exposure duration on the real part of the admittance of the 350°C-dehydrated RTO sample inferred from the values of the measured complex impedance. t_0 denotes the time from the beginning of sample exposure to air. The real part of the admittance of the as-grown RTO sample is depicted in solid black square.

After measuring the 350°C-dehydrated RTO sample inside a glove box, the sample was taken out and dielectric measurements were performed in air during 9 days. The results are presented in Fig. 8 where
165 the real part of the admittivity, inferred from Eq.(3), is depicted as a function of frequency for different air exposure duration. At high frequency, the observation of a plateau indicates a pure conductivity, which value shows a strong decrease from $1,7 \cdot 10^{-4} \text{ S.cm}^{-1}$ at 10^6 Hz for the as-grown RTO ceramic sample (solid black square on Fig. 8) down to $3,6 \cdot 10^{-7} \text{ S.cm}^{-1}$ for the 350°C-dehydrated RTO sample just after exposure to air (open red square on Fig. 8). During the first day of exposure to air, the real part
170 of the admittivity is found to increase rapidly from $3,6 \cdot 10^{-7} \text{ S.cm}^{-1}$ to $9,17 \cdot 10^{-5} \text{ S.cm}^{-1}$. The magnitude of the real part of the admittivity is still increasing from the 3rd to the 6th day reaching a maximum value of $6,1 \cdot 10^{-4} \text{ S.cm}^{-1}$ and then tends to stabilize around the as-grown value.

Nyquist plots for short-time and long-time exposure to air of a 350°C dehydrated RTO sample are presented respectively in the Fig 9 and 10. Nyquist plots were simulated using an equivalent circuit composed by a resistance in parallel with a capacitor, both placed in series with a Warburg impedance which
175 adds a component in $1/\sqrt{i\omega}$ to the equivalent impedance of the simulated system. The coefficient α varies the contribution of the Warburg impedance term in the equivalent impedance of the simulated system. The results of the simulations are shown in Fig. 11 for different values of α . For $\alpha = 0$ (blue curve), a semicircle characteristic of a pure Debye relaxation regime is obtained. For $\alpha = 0.5$ (orange
180 curve), the semi-circle is less well defined and a straight line appears at low frequency. This phenomenon is amplified when the contribution is increased in the Warburg impedance to the equivalent impedance of the simulated system for $\alpha = 1$ (yellow curve). These simulated curves very well reproduce the evolution observed on the Nyquist diagrams of Fig. 9 and 10. It shows that the exposure to air of the 350°C dehydrated sample leads to the emergence of an ionic conduction regime which becomes predominant
185 as the sample rehydrates.

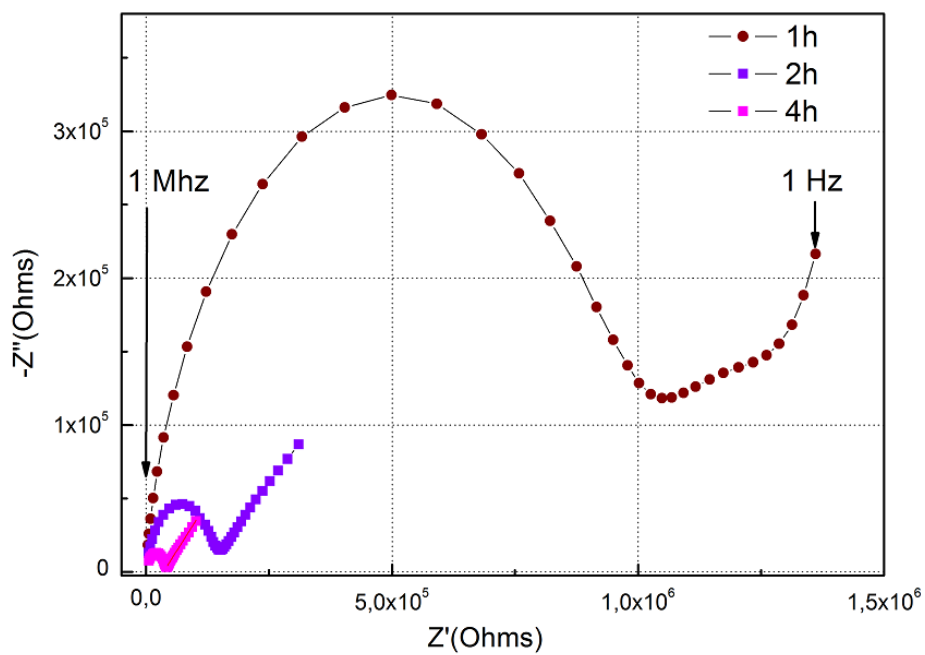


Figure 9: Nyquist plot of one hour to four hours' exposure time of a 350°C dehydrated RTO sample to air.

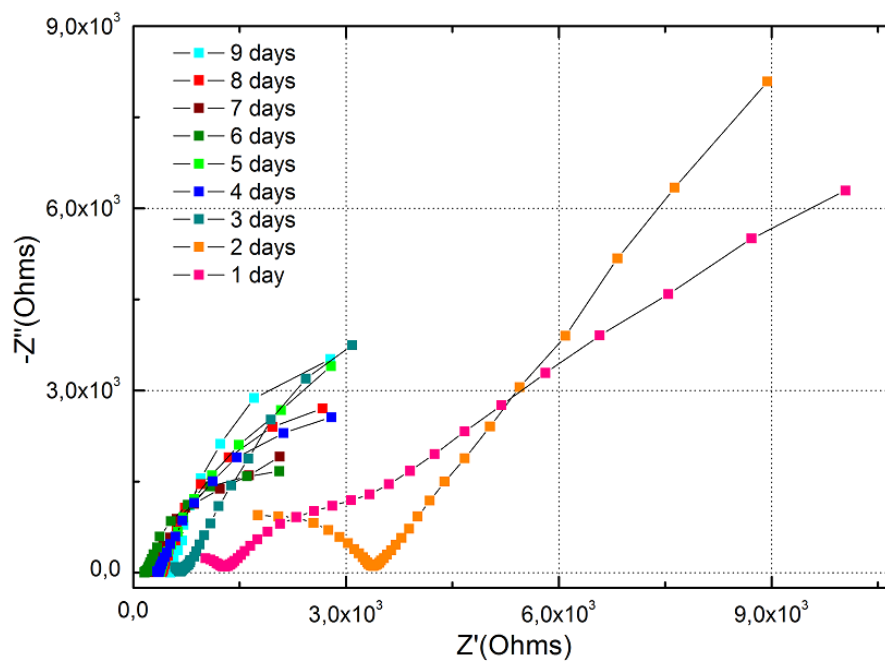


Figure 10: Nyquist plot from one day to nine days' exposure time of a 350°C dehydrated RTO sample to air.

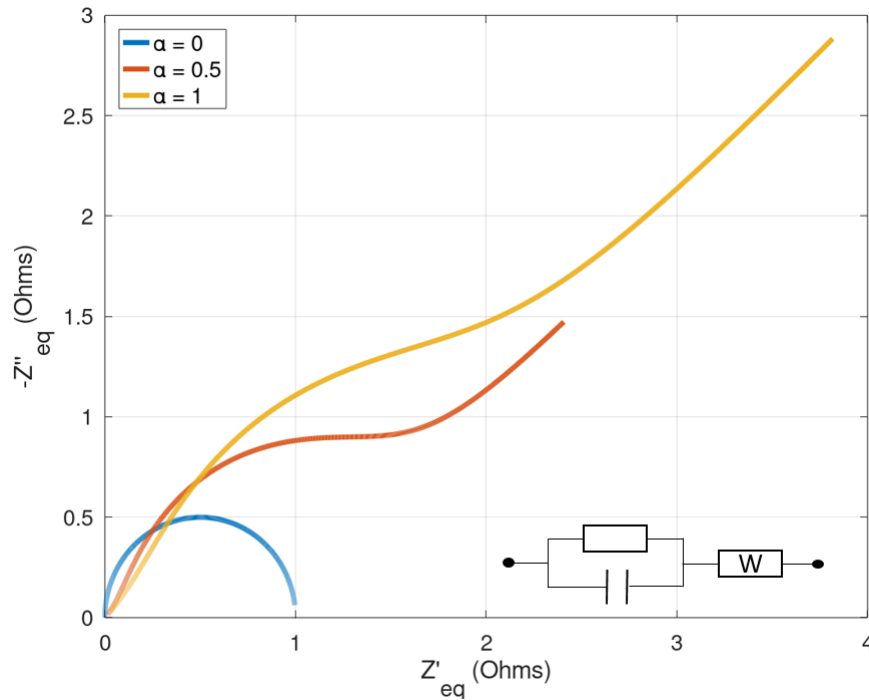


Figure 11: Simulated Nyquist plots obtained for an equivalent circuit composed of a resistance in parallel with a capacitor, both placed in series with a Warburg impedance. A multiplicative factor α varies the contribution of the Warburg impedance term in the equivalent impedance of the simulated system.

2.5. Charge distribution measurements

Charge distributions measurements were performed using the pressure-wave-propagation (PWP) method [17, 18]. The principle of the PWP method is depicted in Fig. 12. This method is based on the propagation of a unipolar short-duration pressure pulse traveling at the velocity of sound through the sample. A high power piezogenerator device is used to generate the pressure pulse which is then transmitted to the sample through a 20-mm aluminum waveguide. As the pressure wave propagates, it induces a slightly local displacement of the charges contained in the material. In short-circuit conditions, the internal current originating from the local charge displacements leads to a current variation in the measurement circuit connecting the electrodes. In open-circuit conditions, it leads to a voltage variation across the electrodes. The obtained signal is therefore an image of the charge distribution in short-circuit conditions or an image of the internal electric field distribution in open-circuit conditions. As the propagation time through the sample is known, the position inside the sample is deduced from the velocity of sound v_s and an image of the electric field convoluted by the pulse width is obtained. See the inset of Fig. 13. All measurements were made at room temperature and under atmospheric pressure.

PWP measurements were performed with several samples by applying a bias voltage ranging from 1 V to 20 V and measuring at the same time the current flowing through the sample. In the experimental measurement setup, there is a 6.5 k Ω resistors in series with the power supply which decreases the effective voltage applied to the sample when current flow through the sample. For a nominal applied voltage

of 1 V, a current of 135 μA is measured, leading in reality to an effective applied voltage across the sam-
 205 ple of 158 mV. For a nominal voltage of 20 V, the effective voltage applied across the sample does not
 exceed 3 V. In such measuring conditions, no decomposition of the material was observed. Furthermore,
 the measurements were found to be entirely reproducible for several successive sets of measurements.
 Of course one expects that in highly hydrated samples, an effective voltage larger than the water disso-
 210 ciation potential (probably modified with respect to pure water) will provoke the electrolysis of water
 but this should not decompose the samples.

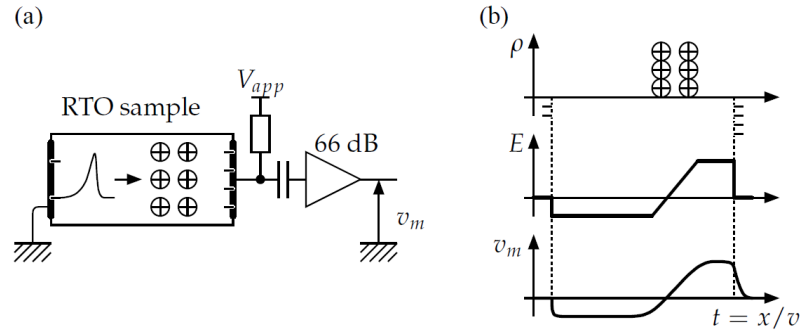


Figure 12: Pressure-Wave-Propagation method principle. a) A pressure pulse is sent through the sample from left to the right. As it propagates, it induces a slight displacement of the charges encountered, which leads to the creation of a current signal in short-circuit conditions or a voltage signal in open-circuit conditions. A continuous voltage V_{app} is applied across the sample during the measurement. b) From top to bottom, charge distribution, electric field distribution and the corresponding measured signal in case of open-circuit conditions.

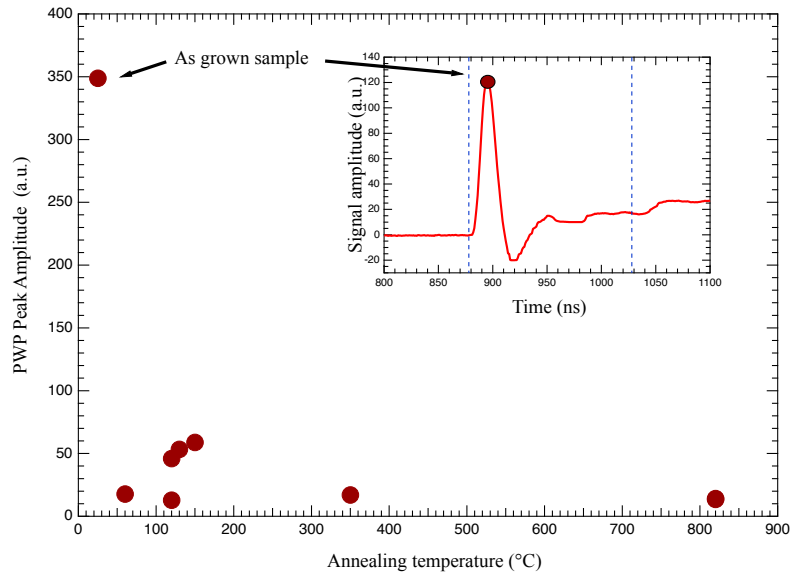


Figure 13: Peak amplitude in the signal measured by PWP method (proportional to the accumulated charge) for a set of RTO ceramic samples dehydrated by annealing under O_2 atmosphere during 4 h at various temperatures. Inset: Typical PWP signal for an as-grown sample under 20 V. The boundaries of the sample are pictured by the blue dotted lines. The peak generated when the pressure pulse enters the sample corresponds to positive charges on the metallic anode (upfront) and negative charges inside the material (downfront). The amplitude of this peak is proportional to the accumulated charge.

Fig. 13 shows the dehydration temperature dependence of the maximum charge distribution signal amplitude for a set of 8 RTO ceramic samples. Each sample was dehydrated at a different temperature during the same duration and the charge distribution was measured for an applied voltage of -20 V using the PWP method. A typical PWP signal is plotted in the inset of Fig. 13 and corresponds to the charge distribution signal amplitude as a function of propagation time for an as-grown sample under 20 V. Similar results were obtained for applied voltages of -1 V, -2 V, -5 V and -10 V. The dotted lines represent the position of the entrance and exit surfaces of the sample.

The peak centered around $t = 900$ ns is signaled by a filled circle. The peak amplitude is extracted for all measured signals and plotted as function of annealing temperature. As reported before in [3, 4], this peak stems from negative ionic carriers accumulated at the anode interface when a negative polarization voltage is applied to the samples. As the pressure probes the induced charge on the anode before the accumulated negative charge in the sample, the peak is positive and proportional to the induced charge quantity, itself proportional to the interface electric field. Because the induced charge on the anode compensate the internal charge, the peak is also directly proportional to the number of negative ionic carriers accumulated inside $Rb_2Ti_2O_5$ near the anode.

2.6. IR absorption measurements

Infrared transmission measurements were carried out in the mid infrared range ($650 - 6000$ cm^{-1}) using a Bruker IFS 66v/S Fourier Transform spectrometer with a HgCdTe (MCT) detector. A globar (SiC) has

been used as source. The spectra obtained at $T = 300$ K is showed in Fig. 14. On this spectrum, one can distinguish a first zone from 650 cm^{-1} to 1000 cm^{-1} covering the energy range where the phonons of the RTO crystal lattice appear, and two other zones corresponding to the vibratory modes of the water molecule around 1400 cm^{-1} and 3000 cm^{-1} . The vibratory mode at 881 cm^{-1} seems to contain two contributions: a broad base related to the apical oxygen phonon bound to titanium in the RTO crystal lattice associated with a thinner peak which could be a vibratory mode attributed to the frustrated libration of an OH hydroxide group. The band around 1400 cm^{-1} and the broad band around 3000 cm^{-1} can be attributed to the vibratory bending and stretching modes of the water molecule, respectively. These measurements therefore make it possible to confirm the coexistence of water in dissociated and molecular form within as-grown samples of RTO.

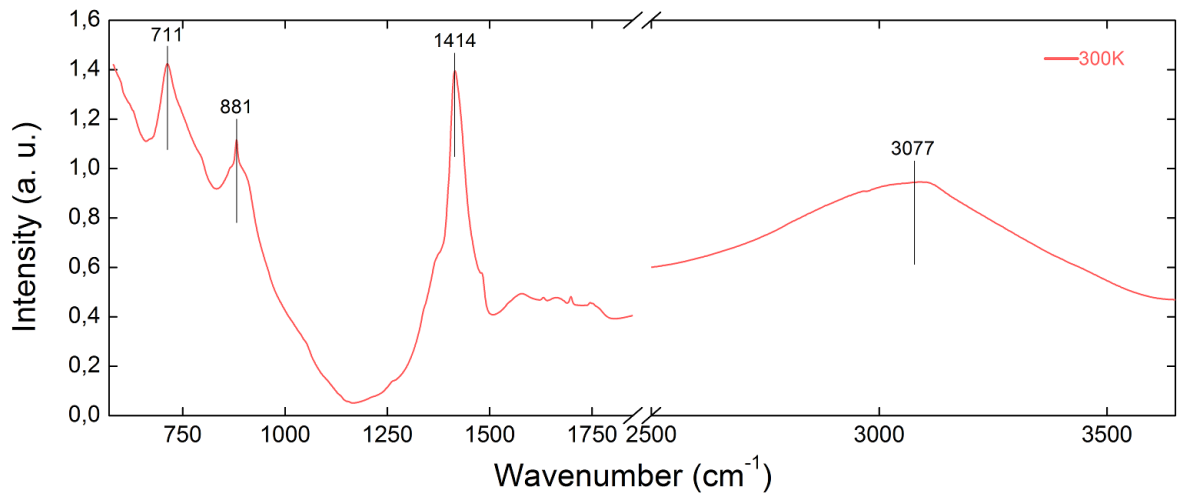


Figure 14: IR spectra acquired on a RTO sample in a KBr matrix at $T = 300$ K.

2.7. Nuclear Magnetic Resonance measurements

In order to have access to local information on the ionic diffusion, NMR spin-lattice relaxation time (T_1) measurements were performed on the ^{87}Rb nucleus which is a sensitive NMR nucleus (high signal intensity). In a nonmagnetic electronic insulator featuring sizable ionic diffusion, it may be expected that the spin-lattice relaxation is dominated by charge fluctuations, such as that caused by hypothetically diffusing Rb^+ ions. In order to test this, T_1 measurements were also performed on the ^{85}Rb isotope. As these two nuclei do not have the same gyromagnetic factor γ and the same quadrupole moment Q , they do not have the same sensitivity to their local spin and charge environment. While the ^{87}Rb nucleus is more sensitive to magnetic fluctuations in the local environment ($[\gamma(^{87}\text{Rb})/\gamma(^{85}\text{Rb})]^2 = 11,5$), the ^{85}Rb nucleus is more sensitive to fluctuations of the electric field gradient ($[Q(^{85}\text{Rb})/Q(^{87}\text{Rb})]^2 = 4,27$). Thus, the isotopic study of T_1 makes it possible to compare (relative weights, temperature dependence) the magnetic and charge relaxation channels, irrespective of their microscopic details.

First of all, the NMR spectrum of ^{87}Rb has to be measured in order to choose the spectral singularity

on which the T_1 will be measured. These measurements were performed on an as-grown RTO powder sample using a Bruker NMR spectrometer ($B_0 = 7$ T) with a low-temperature probe. The ^{87}Rb NMR spectrum, shown in the inset of Fig. 15, was measured at 100 K and obtained by sweeping the frequency
 255 using a spin-echo pulse sequence ($\pi/2 - \tau - \pi$) with a typical τ of 150 μs and a measurement repetition time of 1 s. The spectrum is obtained by combining the Fourier transforms obtained at each frequency.

For an isotope such as ^{87}Rb , with a nuclear spin $I = 3/2$ and a sizable electric quadrupole moment Q , and considering simply the first-order perturbation of the Zeeman Hamiltonian by the interaction between Q and the local electric field gradient, the NMR spectrum will comprise three lines for every
 260 local magnetic/charge environment probed by the 87 rubidium nuclei: one central line separating symmetrically two electric quadrupolar satellites. Due to the electronic insulating nature of RTO, one may expect weak magnetic hyperfine interactions, thus a central line close to the Larmor frequency of ^{87}Rb at the applied 7 T field. Besides, the use of a powder sample will cause an angular distribution of the local magnetic and charge environments, with the main effect being the distribution of the quadrupolar
 265 satellites over a broad frequency range stretching from the central line position up to the largest eigenvalue of the electric quadrupolar tensor. However, the measured spectrum in the inset of Fig. 15 is more complex than such a single "powder distribution". Besides a main distribution with a central line about 98.34 MHz and quadrupolar wings extending at least down to 94 MHz and up to 103 MHz, there is additional signal in the 95-97.5 MHz range. This points to the existence of several locally non equivalent
 270 rubidium sites in this material. In line with the above argument about the expected weak character of the magnetic hyperfine interactions, the T_1 was measured at the singularity of $\nu = 98.34$ MHz, near the Larmor frequency of ^{87}Rb ($\nu_0 = 98.16$ MHz), which belongs to the central line of the majority rubidium site of the material. For the ^{85}Rb isotope, T_1 was measured at the corresponding singularity (in the sense of the ratio of the gyromagnetic ratios) at $\nu = 29.41$ MHz.

275 Since RTO is an electronic insulator, the spin-lattice relaxation time is relatively long, of the order of a few seconds. In order to minimize T_1 measurement time, the progressive saturation method is used [19]. The latter consists in varying the repetition time of the spin echo sequence which allows the system to achieve different degrees of thermal equilibrium recovery between Zeeman levels. Measurements are thus performed purposely out of equilibrium. The magnetization recovery profiles (*i.e.* T_1 values) are
 280 obtained by using Eq.(4) for a spin $I = 3/2$:

$$\frac{M_z(t)}{M_0} = 1 - \frac{\mathcal{A}R(t, T_1)}{5(1 - e^{-6t/T_1}) + \mathcal{A}R(t, T_1)} \quad (4)$$

with $\mathcal{A} = -\frac{1}{2}(\cos\theta - 1)$ where θ is the initial flip angle of the magnetization of the system of nuclear spins and $R(t, T_1) = 10e^{-6t/T_1} + e^{-5t/T_1} + e^{-4t/T_1} + e^{-3t/T_1} + e^{-2t/T_1} + e^{-t/T_1}$. This fit function assumes a relaxation mechanism of magnetic origin, which is improper for the accurate (quantitative) determination of the T_1 value if the relaxation is of electric quadrupolar origin. However, as stated above, the
 285 purpose of these measurements is to characterize the balance of the magnetic and electric quadrupole relaxation channels through comparison of the temperature dependence of the relaxation of the ^{87}Rb

and ^{85}Rb isotopes. For such an assessment, no absolute determination of T_1 is actually needed, but only its relative variation versus temperature.

Fig. 15 displays the comparison between the spin-lattice relaxation rates (T_1^{-1}) of the ^{87}Rb , ^{85}Rb isotopes and the ratio of T_1^{-1} (^{87}Rb) over T_1^{-1} (^{85}Rb) as a function of temperature. The T_1^{-1} measurements exhibit a sizeable increase as expected from the development of ionic diffusion. More surprising is the strong correlation of the data for the two isotopes, which essentially overlap. The fact that the relaxation rates for the two isotopes are comparable in spite of their large difference of sensitivity to the quadrupolar fluctuations shows that the quadrupolar relaxation channel is not overly dominant, contrary to expectations. Note that the quasi-equality of values is itself coincidental, and is sensitive to the choice of fit function. Besides, the constant ratio against temperature shows that the magnetic and quadrupole electric relaxation channels develop in a correlated manner as the temperature increases. This suggests that ionic diffusion is associated to a modification of the local electronic properties of RTO.

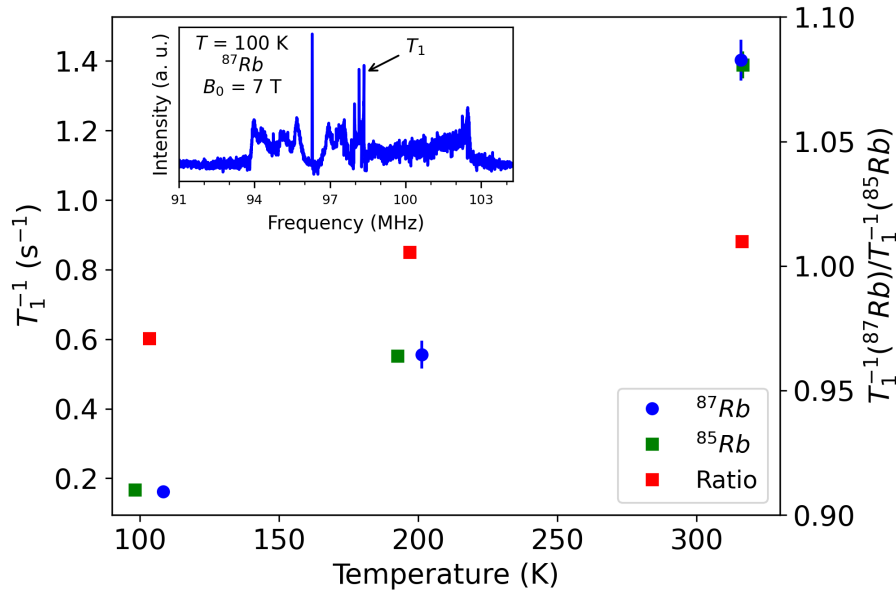


Figure 15: Spin-lattice relaxation rate of the two isotopes of rubidium and of the ratio of T_1^{-1} (^{87}Rb) over T_1^{-1} (^{85}Rb) as a function of temperature.

3. Discussion

TGA clearly indicates that a large amount of water is already incorporated inside as-grown RTO, presumably during the post-synthesis cooling of the crystallites. The dehydration curve of an as-grown sample by heating under oxygen flow exhibits two important mass losses that can be related to water losses. This suggests two distinct types of water binding inside RTO: on the one hand weakly-bound or intercalated water that is completely removed above about 300°C and on the other hand more strongly bound -or dissociated- water which is only eliminated above about 820°C . At 350°C , about

90 % of the water initially present is lost. Based on mass losses obtained from Fig.2, the amount of water initially present in the as-grown material can be estimated. Taking into account the molecular mass of $\text{Rb}_2\text{Ti}_2\text{O}_5$ ($3.86 \text{ g}\cdot\text{cm}^{-3}$), the actual stoichiometry of an as-grown powder formula was therefore $\text{Rb}_2\text{Ti}_2\text{O}_5\cdot(\text{H}_2\text{O})_{0.36\pm 0.071}$. From the rehydration curve (Fig.5), it can be seen that even larger water contents can be reached, with about 0.5 water molecule per formula unit after 96 h of exposure at ambient atmosphere (this value would thus correspond to the measurement labelled "4 days" in Fig. 8). In can be seen in Fig. 5 that the rehydration occurs rapidly, with about 0.08 water molecule incorporated per formula unit after only 2 h of exposure at ambient atmosphere, which correlates with the rapid evolution of the ionic conductivity observed in Fig. 8.

From XRD measurements, it stems that the incorporation of at least more than 0.1 molecule of water per formula unit of $\text{Rb}_2\text{Ti}_2\text{O}_5$ does not lead to a measurable variation of the lattice parameters of RTO, which is surprising and not yet understood. However, since rubidium has a greater steric hindrance, the separation of Ti_2O_5 planes is about 7 \AA which is much larger than for other lamellar oxides such as *i.e.* graphite or vanadium oxides [12, 14]. It might explain that the incorporation of water of size 2.8 \AA occurs at constant lattice parameters.

Dielectric response measurements show a clear water content influence on the evolution of equivalent complex permittivity with respect to frequency. The fact that the complex permittivity of a 350°C -dehydrated sample shifts towards low frequencies points toward the role of water in the implementation of ionic conduction in RTO material. The ionic conduction mechanism and thus the resulting accumulation of charges inside RTO appear to be water-mediated. For a dehydrated sample, the ionic conduction is harder to initiate, explaining the shift towards low frequencies observed in Fig. 7. This hypothesis is confirmed by admittivity measurements presented in Fig. 8. The water incorporation through the 350°C -dehydrated RTO sample leads to an increase of the magnitude of the real part of the admittivity over air exposure time. The same value of the real part of the admittivity as for the as-grown sample is recovered after 3-4 days of exposure to air. In addition, Nyquist plots show that the exposure to air of the 350°C dehydrated sample leads to the emergence of an ionic conduction regime which becomes predominant as the sample rehydrates. These results confirm that the weakly-bound water incorporated within the RTO lattice plays a predominant role on the dielectric properties of the material.

Charge distribution measurements demonstrate that the increase of the dehydration temperature of the RTO samples leads to a strong decrease of the maximum signal amplitude, by a factor up to ~ 24 for RTO samples dehydrated at 820°C (see Fig. 13) compared to as-grown ones. This proves that the number of negative charges accumulated at the anode interface is directly dependent on the water content of the RTO material. Actually most of the signal amplitude (about 95 %) is already lost for a dehydration temperature of 350°C . At this temperature, according to TGA analysis, the adsorbed water is removed at 90 %, which shows that the "weakly-bound" water is essential to the conduction mechanisms.

IR absorption measurements are able to confirm the coexistence of dissociated and molecular water within as-grown RTO samples, in accordance with the hypothesis deduced from the TGA measure-

ments.

The NMR spin-lattice relaxation time measurements highlight the temperature-correlated development
345 of the magnetic and quadrupole electric relaxation channels in the RTO sample. A magnetic diffusive species may explain this result. If this were the case, this would exclude Rb^+ as the diffusive species as it is nonmagnetic. Furthermore, in view of the assumed stoichiometry of RTO, there is no other potential magnetic diffusive species. Another hypothesis could be advanced to explain the experimental observa-
350 tion: valence fluctuations of titanium, which would be correlated in temperature with the appearance of ionic diffusion. In fact, there are some cases of oxide systems in the literature where the valence of the metal cation is modified by the incorporation of water which introduces protons into the material in the form of hydroxide defects [20, 8, 7]. The valence states of the transition metal cations are then reduced in order to preserve the overall electroneutrality of the material. In this second hypothesis and considering the temperature invariance of the measured isotopic T_1 ratio, it can be noted that the proportion of Ti^{3+}
355 ions relative to the proportion of diffusive species does not appreciably change with temperature, if at all. In the opposite case, we would observe a loss of the temperature correlation between the magnetic relaxation channel and the electrical relaxation channel, which is not the case at least up to 310 K. Besides, it is here again possible to exclude Rb^+ as the diffusing species, as it cannot account for a change in valence of the titanium.

360 It is therefore clear from TGA, capacitance and PWP measurements that the number of accumulated ions is highly dependent on the dehydration temperature or the rehydration time and thus on the water content of the samples. This trend is observed both in the maximum amplitude signal and in the conductivity evolution as a function of the dehydration temperature, and is consistent with the overall TGA curve behavior, pointing towards a predominant role of water in the conductivity and the dielec-
365 tric properties of RTO material. A twofold effect of the water content can be envisaged. First the water is responsible for providing ionic charge carriers (proton and hydroxide ions) through dissociation of the water molecule at high temperature during synthesis. These ions can form hydroxide groups attached to the RTO structure, either by adding a proton to an oxygen or by adding replacing an oxygen vacancy by an hydroxide ion. These groups can be rendered mobile by the hopping of protons. Secondly, water
370 molecules are known for favoring both proton and hydroxide mobility through the Grotthuss mechanism [15, 16]. Incorporated water could therefore strongly favor ionic mobility, explaining the high conductivity values that are reported. Through fine tuning of the water content, it may be expected that the high permittivity values are pushed to higher frequencies. In addition, the NMR spin-lattice relaxation time measurements enable to exclude a possible contribution of Rb^+ as the migrating ion and the
375 charge distribution measurements have shown that negative ionic carriers are present near the anode interface. Therefore these ions are presumably hydroxide ions, either by a pure accumulation mechanism through OH^- mobility or by a departure of the H^+ or even by a combination of both mechanisms.

Conclusion

This work demonstrates a strong dependence on the water content of the charge accumulation taking place in the solid electrolyte material $\text{Rb}_2\text{Ti}_2\text{O}_5 \cdot (\text{H}_2\text{O})_x$. The charge distribution signal amplitude inside the material strongly decreases when the dehydration temperature increases, following the trend of the TGA curve. For a dehydration temperature of 350°C , about 95% of the charge accumulation signal in PWP measurements is lost. At this temperature, according to TGA analysis about 90 % of the adsorbed water is removed from the material. It follows that the negative ionic carriers that accumulate in $\text{Rb}_2\text{Ti}_2\text{O}_5$ ceramic samples are hydroxide ions. These results are confirmed by dielectric measurements. The inferred admittivity decreases by almost three orders of magnitude for a sample dehydrated at 350°C , and then quickly recovers after rehydration. IR absorption measurements confirm the presence of molecular and dissociated water in as-grown samples. The NMR measurements allow to exclude that the rubidium ion is the diffusive species within the RTO. The likely microscopical mechanisms are that hydroxide ions and protons are provided by water dissociation, and that incorporated water favors ion conduction through a Grotthuss mechanism associated with a valence change of titanium. This last point is a parameter to explore in order to explain the observed metallic behaviour on the cathode side (the "virtual cathode" creation [3, 4]). Further measurements and simulations studies are ongoing in order to clarify the adsorption and dissociation mechanism of water inside the material, and especially the absence of variation of the RTO cell parameters measured by XRD.

Acknowledgements. The authors gratefully acknowledge investment support from ESPCI Paris. SDSC acknowledges support from Sorbonne Université and RF acknowledges support from French state funds managed by the ANR within the Investissements d'Avenir program under Reference No. ANR-11-IDEX-0004-02 and more specifically within the framework of the Cluster of Excellence MATISSE led by Sorbonne Université. PG wishes to thank Etienne Balan for his help during the IR measurements and for fruitful discussions.

References

- [1] Rémi Federicci, Stéphane Holé, Aurelian Florin Popa, Luc Brohan, Benoît Baptiste, Silvana Merccone, and Brigitte Leridon. $\text{Rb}_2\text{Ti}_2\text{O}_5$: Superionic conductor with colossal dielectric constant. *Physical Review Materials*, aug 2017. 1, 2.4
- [2] Rashmi Rani, Sofia De Sousa Coutinho, Stéphane Holé, and Brigitte Leridon. Colossal dielectric constant in $\text{K}_2\text{Ti}_2\text{O}_5$. *Materials Letters*, 258, January 2020. 1, 2.4
- [3] Sofia De Sousa Coutinho, Rémi Federicci, Brigitte Leridon, and Stéphane Hole. High Ionic Conductivity in the Solid Electrolyte Material $\text{Rb}_2\text{Ti}_2\text{O}_5$. In *2018 IEEE 2nd International Conference on Dielectrics (ICD)*. IEEE, jul 2018. 1, 2.4, 2.5, 3

- [4] Sofia De Sousa Coutinho, Rémi Federicci, Stéphane Holé, and Brigitte Leridon. Virtual cathode induced in $\text{Rb}_2\text{Ti}_2\text{O}_5$ solid electrolyte. *Solid State Ionics*, 333:72–75, may 2019. 1, 2.4, 2.5, 3
- [5] K. Kreuer, E. Schonherr, and J. Maier. Proton and oxygen diffusion in BaCeO_3 based compounds: A combined thermal gravimetric analysis and conductivity study. *Solid State Ionics*, 70-71:278–284, may 1994. 1
415
- [6] Ji Haeng Yu, Jong-Sook Lee, and Joachim Maier. Formation of protonic defects in perovskite-type oxides with redox-active acceptors: case study on Fe-doped SrTiO_3 . *Physical Chemistry Chemical Physics*, 7(20):3560, 2005. 1
- [7] Ji-Haeng Yu, Jong-Sook Lee, and Joachim Maier. Water incorporation in oxides: A moving boundary problem. *Solid State Ionics*, 181(3-4):154–162, feb 2010. 1, 3
420
- [8] N. Bonanos. Oxide-based protonic conductors: point defects and transport properties. *Solid State Ionics*, 145(1-4):265–274, dec 2001. 1, 3
- [9] Ji Haeng Yu, Jong-Sook Lee, and Joachim Maier. Peculiar Nonmonotonic Water Incorporation in Oxides Detected by Local In Situ Optical Absorption Spectroscopy. *Angewandte Chemie International Edition*, 46(47):8992–8994, dec 2007. 1
425
- [10] F.A. Kröger and H.J. Vink. Relations between the concentrations of imperfections in crystalline solids. volume 3 of *Solid State Physics*, pages 307 – 435. Academic Press, 1956. 1
- [11] G. Garcia-Belmonte, V. Kytin, T. Dittrich, and J. Bisquert. Effect of humidity on the ac conductivity of nanoporous TiO_2 . *Journal of Applied Physics*, 94(8):5261, 2003. 1
- [12] Wei Gao, Neelam Singh, Li Song, Zheng Liu, Arava Leela Mohana Reddy, Lijie Ci, Robert Vajtai, Qing Zhang, Bingqing Wei, and Pulickel M. Ajayan. Direct laser writing of micro-supercapacitors on hydrated graphite oxide films. *Nature Nanotechnology*, 6(8):496–500, jul 2011. 1, 3
430
- [13] Yao Yao, Xiangdong Chen, Jinfeng Zhu, Baoqing Zeng, Zuquan Wu, and Xiaoyu Li. The effect of ambient humidity on the electrical properties of graphene oxide films. *Nanoscale Research Letters*, 7:363, 2012. 1
435
- [14] Qiulong Wei, Jin Liu, Wei Feng, Jinzhi Sheng, Xiaocong Tian, Liang He, Qinyou An, and Liqiang Mai. Hydrated vanadium pentoxide with superior sodium storage capacity. *Journal of Materials Chemistry A*, 3(15):8070–8075, 2015. 1, 3
- [15] Noam Agmon. The Grotthuss mechanism. *Chemical Physics Letters*, 244(5-6):456–462, October 1995. 1, 3
440
- [16] Sean T. Roberts, Krupa Ramasesha, Poul B. Petersen, Aritra Mandal, and Andrei Tokmakoff. Proton Transfer in Concentrated Aqueous Hydroxide Visualized Using Ultrafast Infrared Spectroscopy. *The Journal of Physical Chemistry A*, 115(16):3957–3972, April 2011. 1, 3

- [17] S. Hole, T. Ditchi, and A. Lewiner. Non-destructive methods for space charge distribution measurements: what are the differences? *IEEE Transactions on Dielectrics and Electrical Insulation*, 10(4):670–677, 2003. 2.5
- [18] P. Laurenceau, G. Dreyfus, and J. Lewiner. New principle for the determination of potential distributions in dielectrics. *Phys. Rev. Lett.*, 38:46–49, Jan 1977. 2.5
- [19] V. F. Mitrović, E. E. Sigmund, and W. P. Halperin. Progressive saturation NMR relaxation. *Physical Review B*, 64(2), jun 2001. 2.7
- [20] K. D. Kreuer. Aspects of the formation and mobility of protonic charge carriers and the stability of perovskite-type oxides. *Solid State Ionics*, 125(1-4):285–302, oct 1999. 3